Supplement of Atmos. Chem. Phys., 25, 9545–9560, 2025
https://doi.org/10.5194/acp-25-9545-2025-supplement


Atmospheric Chemistry and Physics
Open Access
EGU

*Supplement of*

# Rapid increases in ozone concentrations over the Tibetan Plateau caused by local and non-local factors

**Chenghao Xu et al.**

*Correspondence to:* Jintai Lin (linjt@pku.edu.cn)

**S1 Nested GEOS-Chem simulation setup and scenario design**

We use nested GEOS-Chem simulations over Asia (60°E–150°E, -11°N–55°N) at the native resolution of 0.5° lat. × 0.625° long. to simulate the summertime (June, July and August) ozone change from 2015 to 2019. All nested simulations obtain the boundary conditions of chemicals from the global simulations at 2° lat. × 2.5° long. for the corresponding year. The global and nested simulations are run 6 months and 6 days in advance, respectively, as model spin-up to remove the impact of initial conditions. Compared to the global model setup in Section 2.3, the nested simulations only adjust the $NO_x$ and NMVOC emissions, leaving the rest of the model settings unchanged. To focus on the impacts of emissions and chemical nonlinearity, the meteorological variables to drive the nested model simulations are fixed at the 2015 levels.

For anthropogenic $NO_x$ emissions, we use the emission data in Section 2.4. For anthropogenic VOC emissions, we use the CEDS inventory globally, but used the MEIC (Multi-scale Emissions Inventory of China; www.meicmodel.org) v1.4 inventory (Li et al., 2017; Zheng et al., 2018) for China for VOC species available in MEIC (including acetone, acetaldehyde, lumped C4 + C5 alkanes, ethane, propane, formaldehyde, methyl ethyl ketone, and lumped >= C3 alkenes). As mentioned in Section 2.3, in the VOC emission inventories, local emission sources in the TP region may be substantially underestimated and the emission trends are not accurately accounted for. Chen et al. (2022) found that emissions of many VOC species in the MEIC inventory were underestimated by about an order of magnitude in Lhasa in 2016. Tang et al. (2022) showed a three-fold increase in the concentrations of aromatic and alkane hydrocarbons in the TP urban areas from 2012-2014 to 2020-2022, which were poorly accounted for in the emission inventories. Given the lack of accurate, timely VOC emission data, we adjust the anthropogenic VOC emissions on the TP in the nested simulations as follows. (1) We multiply emissions by a factor of 10 for the VOC species available in MEIC, and by a factor of 2 for other VOC species available in CEDS but not MEIC. The different scaling choice is based on the fact that for the same VOC species available in both CEDS and MEIC, the emissions in CEDS are 4-6 times greater than MEIC over the TP. (2) For alkanes and aromatics, we further account for the emission trends by using the adjusted 2016 emissions in (1) as the baseline, assuming that emissions increased by a factor of three from 2013 to 2021, and assuming that such emission growth was linear.

We conduct multiple simulations to examine the impacts of emission changes on ozone (Table S1). The BASE scenario simulated ozone concentrations in 2015. The E19, NLE19, and LE19 scenarios are used to simulate ozone concentrations as a result of changes in emissions of both $NO_x$ and VOCs in different regions. $NO_x$_E19 and $NO_x$_NLE19 only changed the $NO_x$ emissions in the corresponding regions.

**Table S1:** Detailed descriptions of all scenarios are elaborated in Section S1. Here, LE and NLE are abbreviations for 'Local 1.5º Emission' and 'Non-Local Emission', respectively. Meteorology is fixed at the 2015 level.

| Scenario | $NO_x$ LE year | VOC LE year | $NO_x$ NLE year | VOC NLE year |
|---|---|---|---|---|
| **BASE** | 2015 | 2015 | 2015 | 2015 |
| **E19** | 2019 | 2019 | 2019 | 2019 |
| **NLE19** | 2015 | 2015 | 2019 | 2019 |
| **LE19** | 2019 | 2019 | 2015 | 2015 |
| **$NO_x$_E19** | 2019 | 2015 | 2019 | 2015 |
| **$NO_x$_NLE19** | 2015 | 2015 | 2019 | 2015 |

**Table S2: Changes in averaged ozone mixing ratios over 2015–2019 simulated by the nested GEOS-Chem model.** The results of the averaged ozone mixing ratio change are represented by the mean value and standard deviation of ozone changes in 17 cities.

| Factor | Calculation method | Averaged ozone mixing ratio change [ppb] |
|---|---|---|
| **Emission** | E19 minus BASE | 1.52±0.51 |
| **Non-local emission** | NLE19 minus BASE | 1.21±0.57 |
| **Local emission** | LE19 minus BASE | 0.71±0.37 |
| **$NO_x$ emission** | $NO_x$_E19 minus BASE | 1.34±0.61 |
| **Non-local $NO_x$ emission** | $NO_x$_NLE19 minus BASE | 1.02±0.73 |

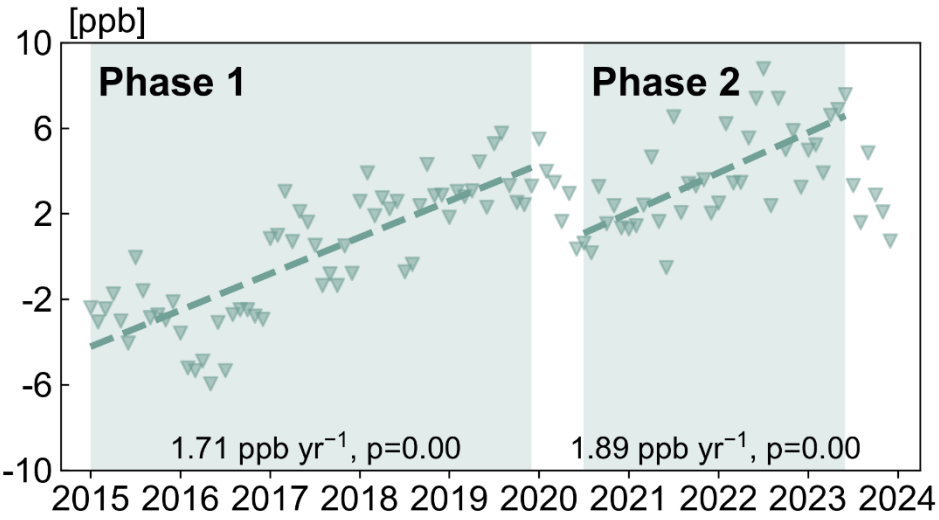


**Figure S1 Monthly variation of deseasonalized MEE ozone mixing ratios averaged over 17 cities on the TP from January 2015 to December 2023. The data points represent the deseasonalized ozone in individual months, and the dashed lines represent the linear regression fit in Phase 1 (from January 2015 to December 2019) and Phase 2 (from July 2020 to June 2023). The slope of linear regression and the p-value are also shown.**

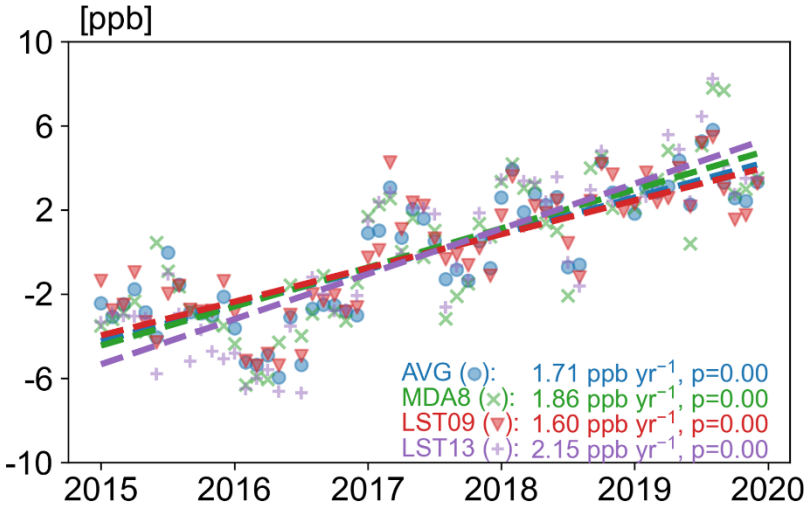


**Figure S2 Monthly variation of deseasonalized MEE ozone mixing ratios averaged over 17 cities on the TP during January 2015 to December 2019. Each color represents an ozone metric, including daily average ozone concentration (AVG), maximum daily 8-h average ozone concentration (MDA8), ozone at 09:00 local solar time (LST09), and ozone at13:00 local solar time (LST13). The**

**data points represent the deseasonalized ozone in individual months, and the dashed line represents the linear regression fit. The slope of linear regression and the p-value are also shown.**

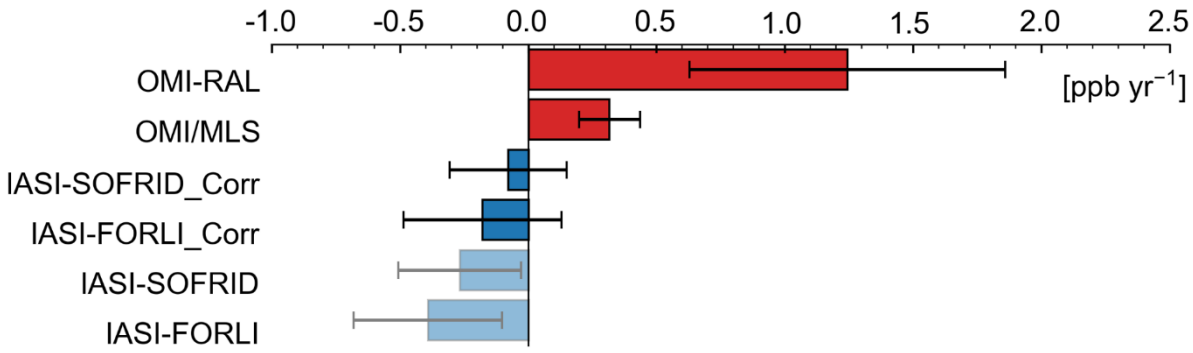


**Figure S3 Trends of deseasonalized tropospheric ozone mixing ratios from 2008 to 2019 based on different satellite datasets. The error bar represents the standard deviation of all gridded data over the TP. The '_Corr' suffix means that the data have been corrected, as described in Section 2.3.**

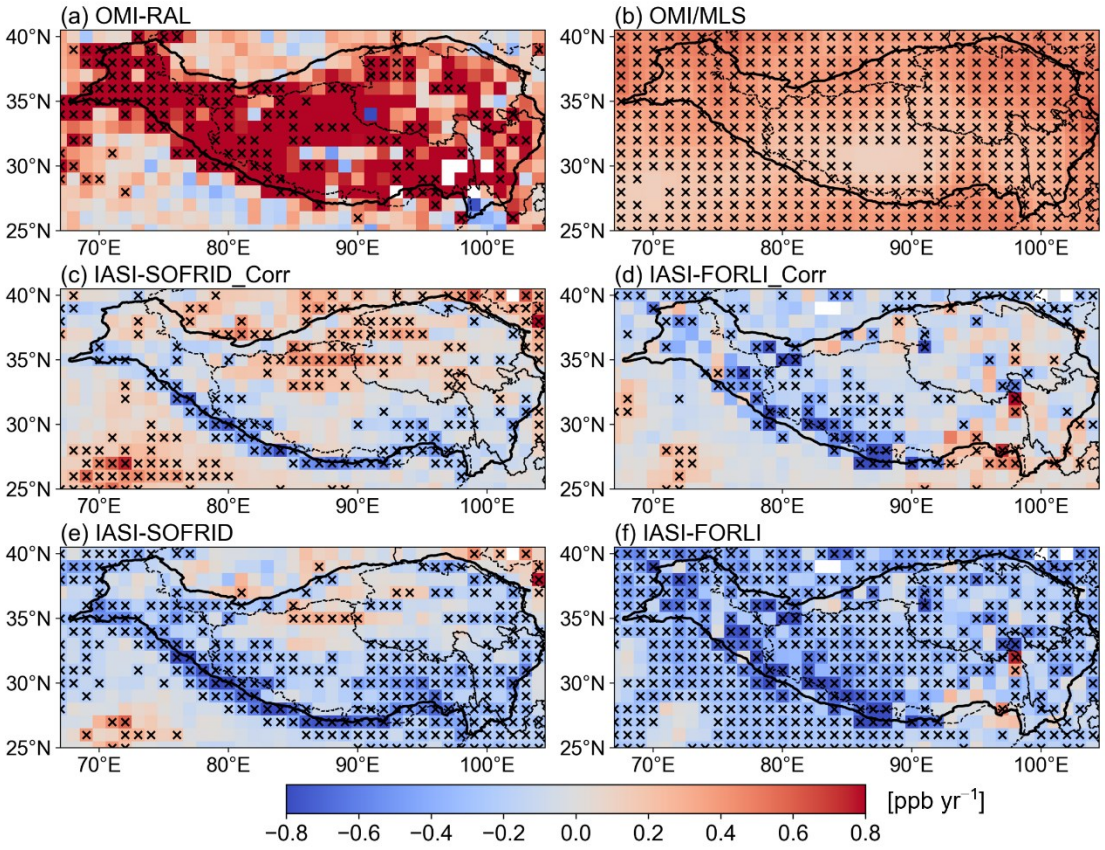


**Figure S4 Spatial distribution of deseasonalized tropospheric ozone mixing ratio trends from 2008 to 2019 for (a) OMI-RAL, (b) OMI/MLS, (c) IASI-SOFRID_Corr, (d) IASI-FORLI_Corr, (e) IASI-SOFRID, and (f) IASI-FORLI. Each cross means the trend in that grid cell is statistically significant (p-value < 0.05).**

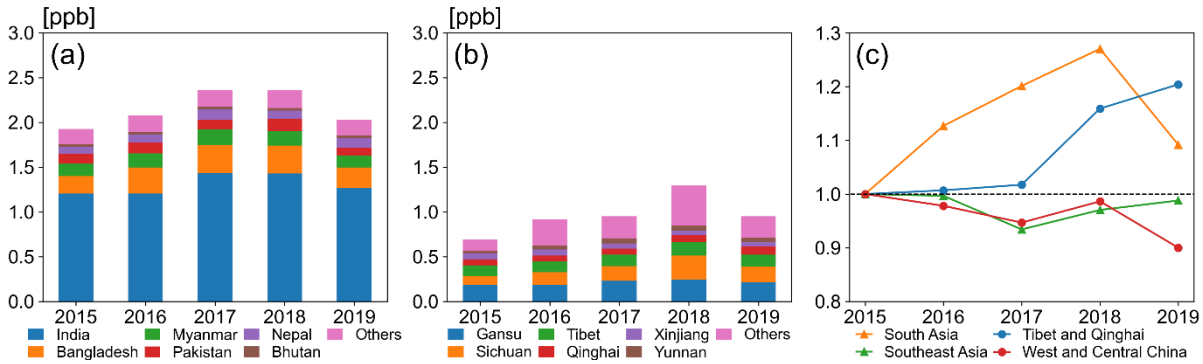


**Figure S5 Annual variation of non-local QNR over 17 cities from (a) foreign countries and (b) provinces of China. Each of the five provinces or countries with the largest average QNR contribution in 2015 is marked with a separate color. (c) Normalized time**

**series of three-year moving average PHLET-OMI NOx anthropogenic emissions in summer for different regions, with summer 2015 emissions as a baseline. Here, the value for 2015 represents the average over 2014–2016, and so on. South Asia includes India, Maldives, Bhutan, Sri Lanka, Pakistan, Bangladesh and Nepal; Southeast Asia includes Philippines, Vietnam, Laos, Cambodia, Myanmar, Thailand, Malaysia, Brunei Darussalam, Singapore, Indonesia, Timor-Leste; and West and Central China includes Inner-Mongolia, Guangxi, Chongqing, Sichuan, Guizhou, Yunnan, Shaanxi, Gansu, Ningxia, Xinjiang, Shanxi, Anhui, Jiangxi, Henan, Hubei, Hunan.**

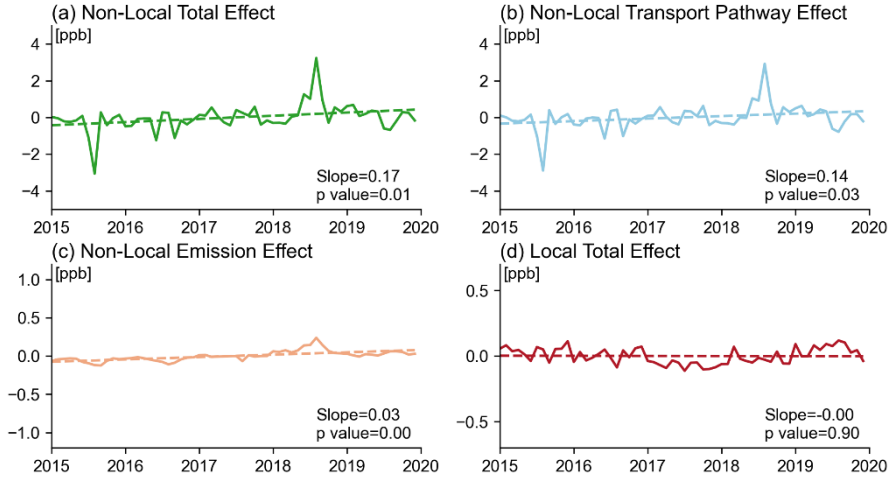


**Figure S6 Deseasonalized monthly variation of QNR at Waliguan. (a) Non-local QNR changes due to the combined effect of changes in anthropogenic emissions and in transport pathway. (b) Non-local QNR changes due to changes in transport pathway alone. (c) Non-local QNR changes due to changes in anthropogenic emissions alone. (d) Local QNR changes due to the combined effect of changes in anthropogenic emissions and in transport pathway.**

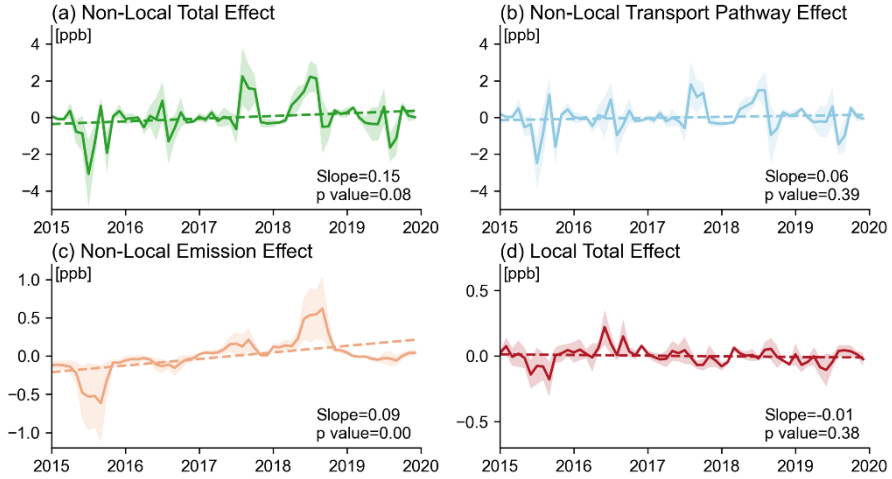

**Figure S7 Deseasonalized monthly variation of QNR over 3 cities (Changdu, Hainan and Lhasa). (a) Non-local QNR changes due to the combined effect of changes in anthropogenic emissions and in transport pathway. (b) Non-local QNR changes due to changes in transport pathway alone. (c) Non-local QNR changes due to changes in anthropogenic emissions alone. (d) Local QNR changes due to the combined effect of changes in anthropogenic emissions and in transport pathway.**

**Reference**


Chen, S., Wang, W., Li, M., Mao, J., Ma, N., Liu, J., Bai, Z., Zhou, L., Wang, X., Bian, J., and Yu, P.: The Contribution of Local Anthropogenic Emissions to Air Pollutants in Lhasa on the Tibetan Plateau, Journal of Geophysical Research: Atmospheres, 127, https://doi.org/10.1029/2021jd036202, 2022.

Li, M., Liu, H., Geng, G., Hong, C., Liu, F., Song, Y., Tong, D., Zheng, B., Cui, H., Man, H., Zhang, Q., and He, K.: Anthropogenic emission inventories in China: a review, National Science Review, 4, 834-866, https://doi.org/10.1093/nsr/nwx150, 2017.

Tang, G., Yao, D., Kang, Y., Liu, Y., Liu, Y., Wang, Y., Bai, Z., Sun, J., Cong, Z., Xin, J., Liu, Z., Zhu, Z., Geng, Y., Wang, L., Li, T., Li, X., Bian, J., and Wang, Y.: The urgent need to control volatile organic compound pollution over the Qinghai-Tibet Plateau, iScience, 25, 105688, https://doi.org/10.1016/j.isci.2022.105688, 2022.

Zheng, B., Tong, D., Li, M., Liu, F., Hong, C., Geng, G., Li, H., Li, X., Peng, L., Qi, J., Yan, L., Zhang, Y., Zhao, H., Zheng, Y., He, K., and Zhang, Q.: Trends in China's anthropogenic emissions since 2010 as the consequence of clean air actions, Atmospheric Chemistry and Physics, 18, 14095-14111, https://doi.org/10.5194/acp-18-14095-2018, 2018.